Progress in Nuclear Energy 194 (2026) 106261

Contents lists available at ScienceDirect

Progress in Nuclear Energy

journal homepage: www.elsevier.com/locate/pnucene

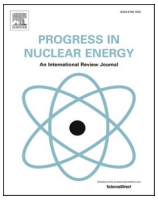

Evaluating local wind circulation metrics for radionuclide transport and dispersion: A practical approach for radiological safety

M.A. Hernández-Ceballos [a,*], M. Sangiorgi [b], N. Conte [b], J.P. Bolívar [c]

[a] Department of Physics, University of Córdoba, Spain
[b] Joint Research Center, Ispra, Italy
[c] Department of Integrated Sciences, Center for Natural Resources, Health and Environment (RENSMA), University of Huelva, Spain

A B S T R A C T

Understanding the atmospheric dispersion and transport of radioactive materials is crucial for assessing radiological exposure and potential health risks, as well as for optimizing radiological environmental impact assessment and radiological monitoring networks. The dispersion of radionuclides following an accidental release from a nuclear facility is highly influenced by local wind circulation patterns, yet these effects are often overlooked in routine atmospheric dispersion assessments. This study evaluates the role of simple wind circulation indices—stagnation, recirculation, and ventilation—in shaping the dispersion of radioactive material, demonstrating their relevance for nuclear safety planning. The analysis focuses on the Almaraz Nuclear Power Plant (ANPP), where 1.256 atmospheric dispersion simulations were conducted using the RIMPUFF model over a four-year period (2012–2015) under different meteorological conditions. Considering the existing set of 84 monitoring stations included in the EURDEP system in an area of 200 km around the ANPP, the influence of each local atmospheric process is analyzed and characterized by taking the TGDR maximum values reached, and the number of monitoring stations affected in each simulation. On average, results demonstrate that high stagnation confines radionuclide plumes near the source, with maximum TGDR reaching 0.005 μSv/h and affecting up to 14 monitoring stations. In contrast, high recirculation enhances local accumulation, leading to, on average, peaks of 0.035 μSv/h and reducing the number of stations impacted (12 monitoring stations). High ventilation conditions promote wider dispersion, with maximum TGDR of 0.002 μSv/h affecting 10 monitoring stations. Extreme cases of each atmospheric process are also analyzed, showing distinct effects on the spatial distribution of affected monitoring stations. These findings highlight that wind circulation indices, derived from routine meteorological data, offer a straightforward yet effective means of anticipating dispersion behaviour in emergency scenarios.

1. Introduction

Meteorological conditions are fundamental in understanding and assessing the dispersion of radionuclides in the atmosphere, as they directly govern the transport and deposition processes of radioactive materials (e.g., von Schoenberg et al., 2021; Nabavi et al., 2023). Conducting a comprehensive radiological environmental impact assessment requires a thorough characterization of meteorological variables, given their strong influence on airborne contaminant behaviour (IAEA, 2018). Key factors such as wind speed and direction, atmospheric stability, temperature gradients, and precipitation patterns determine how radionuclides move and settle after their release (e.g., Birikorang et al., 2015; Elkhatib et al., 2021). In particular, wind dynamics play a decisive role in shaping the trajectory and dilution of radioactive plumes (e.g., Yoshikane et al., 2016; Choi et al., 2023). High wind speeds can enhance dispersion and reduce radionuclide concentrations near the ground, whereas low wind speeds may contribute to localized accumulation and prolonged contamination (e.g., Pinheiro et al., 2017; He et al., 2024). Additionally, diurnal variations in wind patterns introduce spatial and temporal fluctuations in airborne radioactivity levels, with orographic features—such as mountains and valleys—further modulating local wind regimes. Given these influences, understanding both regional and site-specific wind circulation is essential for accurately predicting variations in radionuclide concentrations within a given area (e.g., Yoshikane and Yoshimura, 2018; Huang et al., 2023).

To analyze and quantify these effects, it is necessary to characterize local wind behaviour using appropriate methodologies. Several approaches exist for this purpose, including advanced atmospheric modeling tools such as the Weather Research and Forecasting (WRF) model (García-Santiago et al., 2024), as well as statistical evaluations of observational datasets (Adame et al., 2009). A well-established yet computationally simple method was developed by Allwine and Whiteman (1994) to describe the impact of horizontal wind flow on pollutant transport by distinguishing between stagnation, recirculation, and ventilation conditions. Recirculation processes can trap radionuclides in specific areas, leading to extended exposure times, whereas ventilation mechanisms enhance atmospheric dispersion and facilitate the removal of contaminants from the region. Stagnation, on the other hand, occurs

* Corresponding author.
E-mail address: f92hecem@uco.es (M.A. Hernández-Ceballos).

https://doi.org/10.1016/j.pnucene.2026.106261
Received 7 March 2025; Received in revised form 24 November 2025; Accepted 11 January 2026
Available online 1 February 2026

when low wind speeds limit dispersion, resulting in radionuclide accumulation. Although this methodology assumes homogeneous wind conditions and presents some limitations, its ease of application—relying solely on hourly wind data—has led to its widespread use worldwide (e.g., Levy et al., 2010; Wang et al., 2022). However, despite its extensive application in air quality studies, this is the first time it has been employed to characterize radionuclide dispersion and assessed for its relevance in radiological environmental impact assessments.

The primary objective of this study is to evaluate how local wind circulation patterns influence the spatial and temporal variability of radionuclide concentrations following a potential release from a nuclear power plant (NPP). To achieve this, the methodology developed by Allwine and Whiteman (1994) is used as a reference for quantifying and classifying recirculation, ventilation, and stagnation conditions in the study area. These wind regimes are further analyzed using hourly wind speed and direction data to characterize their daily variability and assess their impact on near-surface transport processes. The influence of each atmospheric process on radionuclide dispersion is then examined by correlating the wind regime classifications with RIMPUFF dispersion model simulations (Thykier-Nielsen et al., 1999), which simulate the spread of radioactive material from the NPP. In general, the following research topics are aimed to:

- Characterize stagnation, recirculation, and ventilation patterns in an area potentially affected by a radiological release.
- Assess the role of surface wind dynamics in radionuclide dispersion, considering parameters such as the number of affected monitoring stations, and peak values.
- Analyze and compare the atmospheric dispersion of radionuclides during extreme conditions associated with each wind regime.

To conduct this study, the Almaraz Nuclear Power Plant (ANPP) was selected as the reference site, with the analysis covering the period 2012–2015 (Sangiorgi et al., 2023). The structure of the paper is as follows: Section 2 outlines the methodology and data sources, Section 3 provides details on the case study, while Section 4 presents and discusses the obtained results. Finally, Section 5 summarizes the main conclusions of the study.

2. Horizontal wind characterization at the release site

To assess the influence of local wind patterns on radionuclide dispersion, we characterized horizontal wind conditions at the emission site by computing key transport indicators. This approach, adapted from previous methodologies on atmospheric flow classification (Allwine and Whiteman, 1994; Russo et al., 2018) relies on three primary parameters: the net transport distance (L), the total wind run (S), and the recirculation factor (R) (Fig. 1). In this study, the indicators were calculated for the period 2012–2015 at the release site using hourly wind data (direction and speed) extracted from ERA5 (Hersbach et al., 2020), the fifth-generation global reanalysis produced by the European Centre for Medium-Range Weather Forecasts (ECMWF). ERA5 is a major upgrade over ERA-Interim, using a more advanced data-assimilation system and a much larger set of observations, especially satellite data, to better reconstruct past atmospheric conditions, and it provides hourly atmospheric fields at about 31 km horizontal resolution on 137 vertical levels up to 0.01 hPa. In our case, we use hourly ERA5 data on a regular 0.25° × 0.25° latitude–longitude grid; when requested in NetCDF format, these data are re-gridded so that continuous parameters are interpolated using bilinear interpolation and discrete parameters using nearest-neighbour, while in time the fields are taken directly at the available hourly (HRES) timestamps without additional temporal interpolation. More information can be consulted in https://cds.climate.copernicus.eu/datasets/reanalysis-era5-single-levels?tab=overview.

For each hourly wind observation, the wind vector ($\vec{V}$) was decomposed into its east-west (u) and north-south (v) components, allowing the following calculations:

$$\overline{V}_i = (u_i, v_i) \; where \; i = 1, 2, \ldots N$$

where N represents the total number of observations in the dataset.

The net transport distance (L) is defined as the magnitude of the displacement of an air parcel over a specified time interval (τ), which is this study is set to 24 h to capture daily-scale transport patterns, and it is computed as:

$$L_{i\tau} = T\left|\sum_{j=1}^{i-\tau+1} \overline{V}_j\right|$$

in contrast, the total wind run (S) quantifies the absolute distance travelled by the air parcel over the same period, regardless of direction:

$$S_{i\tau} = T\sum_{j=1}^{i-\tau+1} |\overline{V}_j|$$

where T represents the time interval between consecutive observations (1 h in this study).

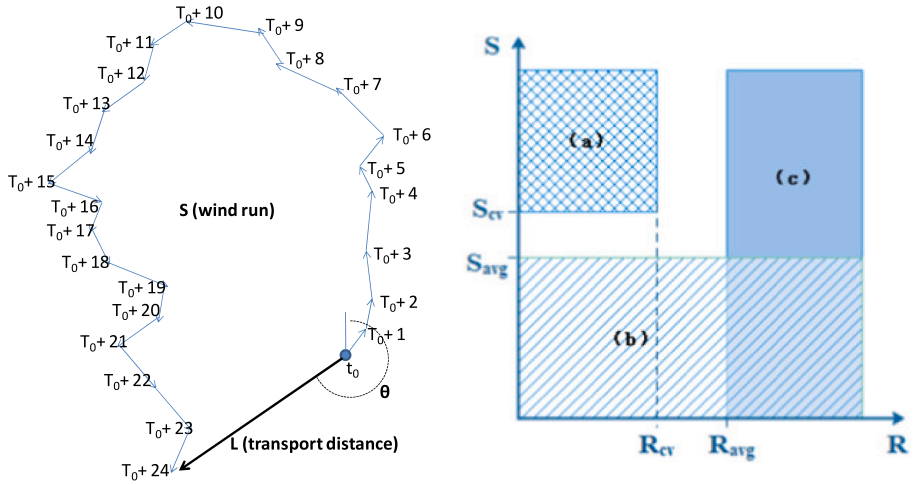

Fig. 1. a) Illustration of the definitions of win run (S) and transport distance (L) assuming a 24-h transport time and 1-h-average observations; b) Classification of local wind fields according to: (a) ventilation, (b) stagnation, (c) recirculation criteria. The overlap in (b) and (c) represents simultaneous stagnation and recirculation (Zhou et al., 2019).

Finally, the recirculation factor (R) is then determined as:

$$R_{it} = 1 - \frac{L_{it}}{S_{it}}$$

This dimensionless parameter ranges from 0 to 1, where values close to zero indicate a unidirectional wind flow with minimal recirculation, while values approaching one suggest strong recirculation and negligible net displacement.

Using these indicators, each single calculated value was classified into one of three wind transport regimes based on predefined thresholds. The classification criteria, following Russo et al. (2018) and for the period 2012–2015, are as follows (Fig. 1b):

- **Stagnation:** $S_{it} \leq S_{avg}$, indicating conditions where weak winds limit transport efficiency, potentially leading to localized accumulation of airborne substances. S_{avg} means the average value of S over the period 2012–2015.
- **Recirculation:** $R_{it} \geq R_{avg}$, characterizing scenarios where the wind undergoes directional shifts, reducing the net displacement of air parcels and promoting local retention. R_{avg} means the average value of R over the period 2012–2015.
- **Ventilation:** $S_{it} \geq S_{cv}$ *and* $R_{it} \leq R_{cv}$, where S_{cv} and R_{cv} correspond to the 75th and 25th percentiles of the respective variables, indicating conditions that favor dispersion and pollutant dilution.

3. Case study

The study focuses on the Almaraz Nuclear Power Plant (ANPP), located in western Spain and near the Portuguese border. The region's topography is characterized by the Tajo River valley, flanked by mountain ranges reaching approximately 1000 m above sea level. This topography significantly influences local wind patterns, channelling winds predominantly along the west-east axis through the valley (Fig. 2b), with clear seasonal variations. In winter, wind frequencies are more evenly distributed among the primary directions, while spring shows a slight enhancement in westerly winds. Summer exhibits the most pronounced dominance of westerly winds, with low wind speed, while autumn closely mirrors the overall annual pattern but with slightly increased in frequency and intensity in the easterly winds. Across all seasons, wind speeds predominantly range between 1.0 and 4.0 m/s, with higher speed classes (≥4.0 m/s) in winter and spring.

To simulate the atmospheric dispersion of radionuclides in the event of an accidental release, we used the RIMPUFF dispersion model within the JRODOS decision support system. The meteorological boundary conditions for RIMPUFF are provided by the Global Forecast System analysis (GFS-ANL) produced by the National Centers for Environmental Prediction (NCEP), obtained from the NOMADS portal. These data have a temporal resolution of 6 h and a horizontal grid spacing of 0.5° (approximately 55 km), and they span the 1000–10 hPa pressure range on 26 standard levels. The choice of this dataset is primarily motivated by its free availability and the possibility of extending future analyses using a consistent set of meteorological inputs. The JRODOS meteorological preprocessor (Andronopoulos et al., 2010; Kovalets et al., 2013) ingests these fields, performs spatial interpolation onto the model grid, and applies a wind-field adjustment procedure to the interpolated wind components to ensure mass-conserving flow. The simulations represent a hypothetical large-break loss of coolant accident (LBLOCA), resulting in the release of 1.1×10^{12} Bq of radioactive material over a 24-h period. The emitted radionuclides include Iodine-131, Cesium-137, and Strontium-90, with an initial peak release occurring in the first hour (Sangiorgi et al., 2023), ensuring that the time-dependent emission profile is fully represented in the dispersion simulations.

To ensure comprehensive coverage of different atmospheric conditions, 1.256 independent simulations were conducted over the period 2012–2015, each initialized daily. For more detailed information, readers can refer to the original article by Sangiorgi et al. (2023). Simulations were seasonally distributed, with 329 in winter (December, January, February), 314 in spring (March, April, May), 297 in summer (June, July, August), and 316 in autumn (September, November, December). The computational domain covered a 200 km × 200 km

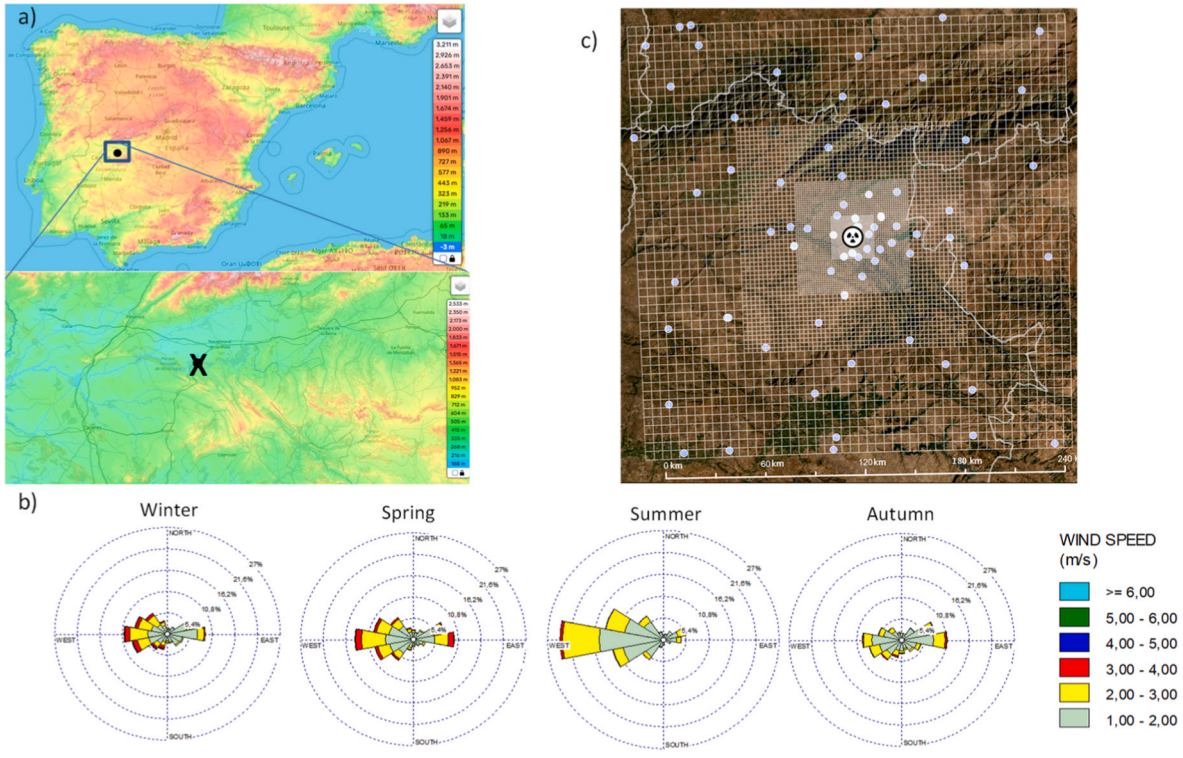

Fig. 2. a) Location of the Almaraz NPP, b) total and seasonal wind roses during the period 2012–2015, and c) the locations of the ANPP, and EURDEP stations in the simulation domain.

region surrounding ANPP, incorporating 84 radiological monitoring stations from the EURDEP (European Radiological Data Exchange Platform) network (Sangiorgi et al., 2020; https://remon.jrc.ec.europa.eu/About/Rad-Data-Exchange). Although these stations are not uniformly distributed, their capability to detect potential radioactive plumes has been previously assessed (Sangiorgi et al., 2023), and they represent the actual operational monitoring network in the region. This configuration is therefore considered suitable for the objectives of the present study.

Hourly time series of Total Gamma Dose Rate (TGDR) over the first 24 h after each release were obtained at each one of the 84 monitoring stations. This time of 24 h is necessary to be consistent with the calculation of surface wind parameters (section 2.1). For the present analysis, we applied a threshold of 100 nSv/h and excluded all values falling below this limit (Hernández-Ceballos et al., 2023; Sangiorgi et al., 2023). This relatively high threshold is consistent with the requirement to remove the natural background contribution and to reduce the likelihood of false radiological alarms, for example those related to short-term radon enhancements (Cinelli et al., 2014). Therefore, a monitoring station was classified as affected only when its simulated TGDR exceeded 100 nSv/h within the first 24 h. To assess the influence of atmospheric conditions on radionuclide dispersion, we analyzed several key dispersion metrics. These include the number of affected monitoring stations, the maximum TGDR recorded at any simulation (Max_Max, in nSv/h), and the distance from the source to the location where this maximum occurred (Max_Dis, in km). Additionally, the average of the maximum TGDR recorded across all affected stations (Max_Avg, in nSv/h) was calculated to assess overall dispersion intensity. Finally, the number of stations impacted (Station) and the farthest station impacted by each simulated plume (Station_Far) were identified.

4. Results and discussion

4.1. Wind field classification

The daily trace of wind run (S) and recirculation (R) factor during the period 2012–2015, and considering a $\tau = 24$ h, is presented in Fig. 3. Considering the method suggested by Russo et al. (2018), the critical transport indices (CTIs) were: $S_{avg} = 233$ km (green line); S (P_{75}) = 281 km; S (P_{25}) = 168 km, $R_{avg} = 0.16$ (red line); R (P_{75}) = 0.22; R (P_{25}) = 0.03. Assuming these thresholds, there was a dominance of events classified as stagnation (57 %, below S_{avg}), whilst there was a lower occurrence of recirculation (33 %, above R_{avg}). During this period, there was a small occurrence of ventilation (14 %, within blue lines), while the combination of stagnation and recirculation processes reached the 29 % (below S_{avg} and above R_{avg}).

Fig. 4a displays the monthly variation (in frequency) of ventilation, recirculation, stagnation, and combined stagnation-recirculation processes during the period 2012–2015. Ventilation days exhibit a pronounced seasonal trend, with the highest frequency observed in March (approximately 18 %) and the lowest in September–October (around 3 %), reflecting enhanced atmospheric ventilation in late winter and early spring, in agreement with the highest wind speed values reached in this period (Fig. 2b). These results are expected, due to the interaction of several meteorological systems brings more instability, causing higher wind speeds (AEMET, 2019). In contrast, recirculation and stagnation days show less pronounced seasonality, with frequencies ranging between 5 % and 10 % throughout the year, with slight peaks during summer months, and a decrease in June. Combined stagnation-recirculation days also showed moderate monthly stability, with a marginal increase in December. Although ERA5 data at 0.25° resolution cannot explicitly resolve mesoscale circulations such as slope winds or channeling, the general influence of the valley orography on regional wind patterns is still reflected in the broader-scale flow. These findings, therefore, suggest a marked seasonal modulation of ventilation processes, driven likely by synoptic-scale meteorology, while recirculation and stagnation are more persistent phenomena, with limited variability over the year.

To complement this analysis, Fig. 4b shows the monthly averages of stagnation distance (S, in kilometers) and the recirculation factor (R, dimensionless). The uncertainty of each one is provided as the standard error of the mean ($Sx/N^{1/2}$, being Sx the standard deviation and N the number of values summarized in the average). While S distances remain consistently high throughout the year, with averages exceeding 200 km and a total average of 235 km, peaking slightly in February–March, as well as, in November. This trend indicates effective atmospheric transport during most months, particularly in transitional seasons (spring and autumn). In contrast, the recirculation factor displays an inverse seasonal behaviour, with higher values in late summer (maximum in September, approximately 0.22) and lower values in winter and spring. The observed inverse relationship between stagnation distance and the

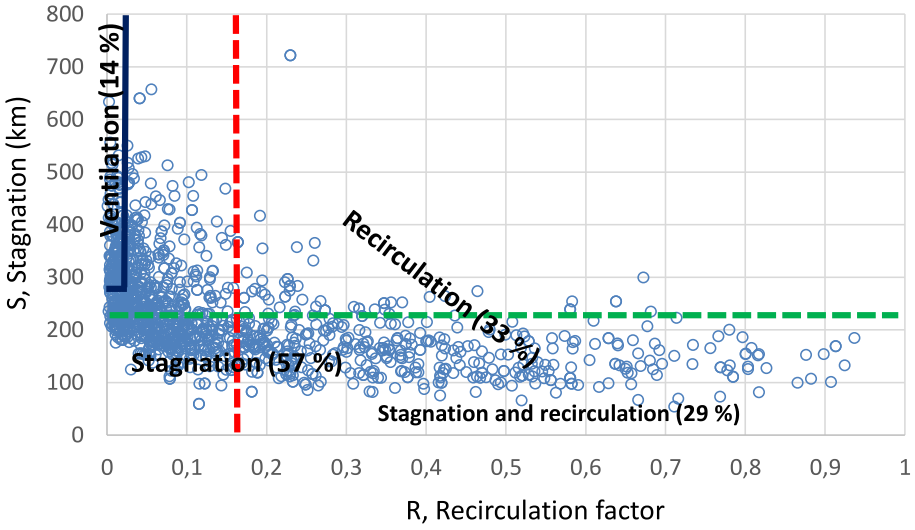

Fig. 3. Classification of local wind fields according to ventilation, stagnation, and recirculation criteria for the historical period 2012–2015. Each point represents the daily trace of each parameter. The critical transport indices determined for the airshed are, red- and green-dashed lines indicate, respectively, S_{avg} and R_{avg}; and the blue lines indicate the 75th and 25th percentile points of S (horizontal) and R (vertical), respectively. (For interpretation of the references to colour in this figure legend, the reader is referred to the Web version of this article.)

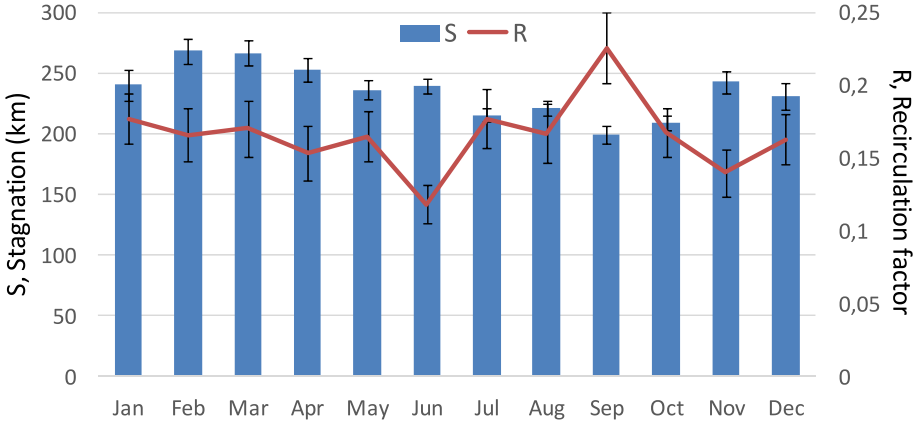

Fig. 4. a) Monthly variation (in frequency) of ventilation, recirculation, stagnation, and combined stagnation-recirculation processes, and b) monthly averages of stagnation distance and the recirculation factor.

recirculation factor highlights a seasonal interplay, where stronger atmospheric mixing and transport in spring and autumn are countered by increased recirculation and weaker air exchange during summer months. Therefore, according to this analysis (period 2012–2015), this area seems to be prone to ventilation events in Winter/early spring, and more stagnation/recirculation events in summer.

4.2. *Characterization of horizontal flows: daily cycles*

Fig. 5 displays surface wind patterns and hourly wind evolution for ventilation and recirculation scenarios at the study site. During ventilation days the wind rose reveals a predominant westerly wind direction, with wind speeds generally exceeding 4 km/h. On average, the diurnal variation shows a steady wind coming from the west throughout the day, while wind speed increases gradually from morning to peak values (8 km/h) around late afternoon (16:00–18:00) before declining in the evening. In contrast, recirculation days exhibit changes in wind direction, as indicated by the wind rose, with significant contributions from the west and east, as well as a notable proportion of lower wind speeds (<4 km/h). The hourly evolution of surface winds indicates a marked variability in wind direction, with shifts from westerly during the night to easterly during the morning, and westerly again during the afternoon. Wind speed remains consistently low, peaking slightly around midday (12:00–14:00) but not exceeding 4–6 km/h.

These local atmospheric dynamics are closely related to the location of the ANPP within the west-east oriented valley, which channels the predominant westerly fast winds during ventilation scenarios, and the development of mesoscale circulations under recirculation processes, driven by diurnal heating and cooling cycles, contributes to the variability in wind direction and lower wind speeds characteristic of

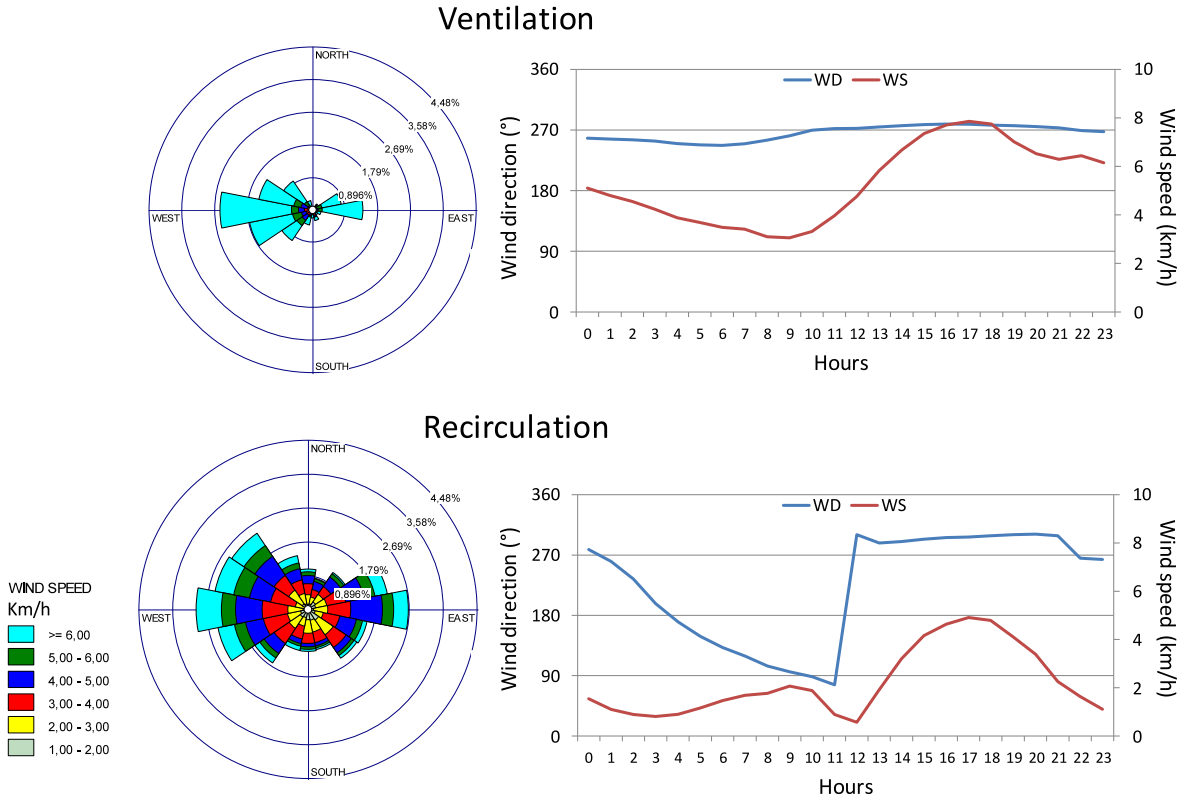

Fig. 5. Wind rose and daily surface wind dynamics during ventilation and recirculation processes. WD: Wind direction, WS: Wind speed.

recirculation days (e.g., Wu et al., 2021). These mesoscale processes, combined with the valley's topographic influence, play a crucial role in modulating surface wind patterns and their impact on pollutant dispersion in the region.

4.3. Atmospheric dispersion of radionuclides and wind flow dynamics

Here, we compare the influence of the ventilation, stagnation and recirculation processes on the atmospheric dispersion parameters defined in section 2.3, based on the results of 1256 regional scale atmospheric dispersion simulation of accidental emission of radionuclides from the ANPP. To address this analysis, we have firstly associated the starting time of each simulation with the corresponding classification of local wind fields at that time (ventilation, stagnation, recirculation) (see section 2.1). Hence, Fig. 6 illustrates, on average, the impact of stagnation, recirculation, and ventilation on radionuclide dispersion by comparing their presence and absence across five key parameters (section 3.1): Max_Avg, Max_Max, Max_Dis, Stations, and Station_Max. Different averages are then calculated, and the uncertainty of each one is provided as the standard error of the mean ($Sx/N^{1/2}$, being Sx the standard deviation and N the number of values summarized in the average).

The results indicate that stagnation and recirculation lead to increase the quantity of GDR. On average, stagnation results in a GDR at about 0.005 μSv/h, whereas under no stagnation conditions, this value is lower (0.003 μSv/h). A similar behaviour is observed for Max_Max, where stagnation leads to a peak GDR close to 0.031 μSv/h compared to a reduced value under no stagnation (0.017 μSv/h). Recirculation exhibits the same pattern, with Max_Avg values slightly above 0.005 μSv/h and Max_Max peaking near 0.035 μSv/h, confirming the role of these processes in radionuclide accumulation. In the case of ventilation process, Max_Avg and Max_Max values were higher under non-ventilation conditions (0.002 μSv/h and 0.011 μSv/h, respectively), although, yet lower than in stagnation or recirculation cases, indicating that ventilation processes promote broader dispersion.

This figure also shows, on average, that the distance of the maximum GDR (Max_Dis) presents minor differences across scenarios, with values remaining below 20 km, and lower in the case of stagnation and recirculation processes, and higher in the case of ventilation process. This result, in general, clearly suggests that while dispersion occurs, the highest radioactivity values are limited in extent. The number of affected monitoring stations (Stations) also follows a clear behaviour: stagnation and recirculation increase the number of impacted stations to around 25, whereas under no stagnation or no recirculation conditions, this value is reduced to below 20. Ventilation, in contrast, leads to an even lower number of affected stations (15), reinforcing its role in radioactive dilution. Finally, the Station_Far parameter remains consistently high across all conditions, with the farthest affected station located at similar distances regardless of the scenario. This suggests that, although local circulation patterns such as stagnation and recirculation favor accumulation and ventilation enhance dispersion, emissions are not confined to a purely local environment and can still reach a large number of stations, even if the recorded values are lower. Overall, these findings confirm that stagnation and recirculation promote the accumulation and persistence of radionuclides, whereas ventilation enhances dispersion and minimizes localized accumulation. This analysis underscores the critical role of meteorological conditions in radionuclide dispersion and highlights the need to incorporate these parameters into environmental impact assessments.

Finally, Fig. 7 reveals distinct correlations between the dispersion

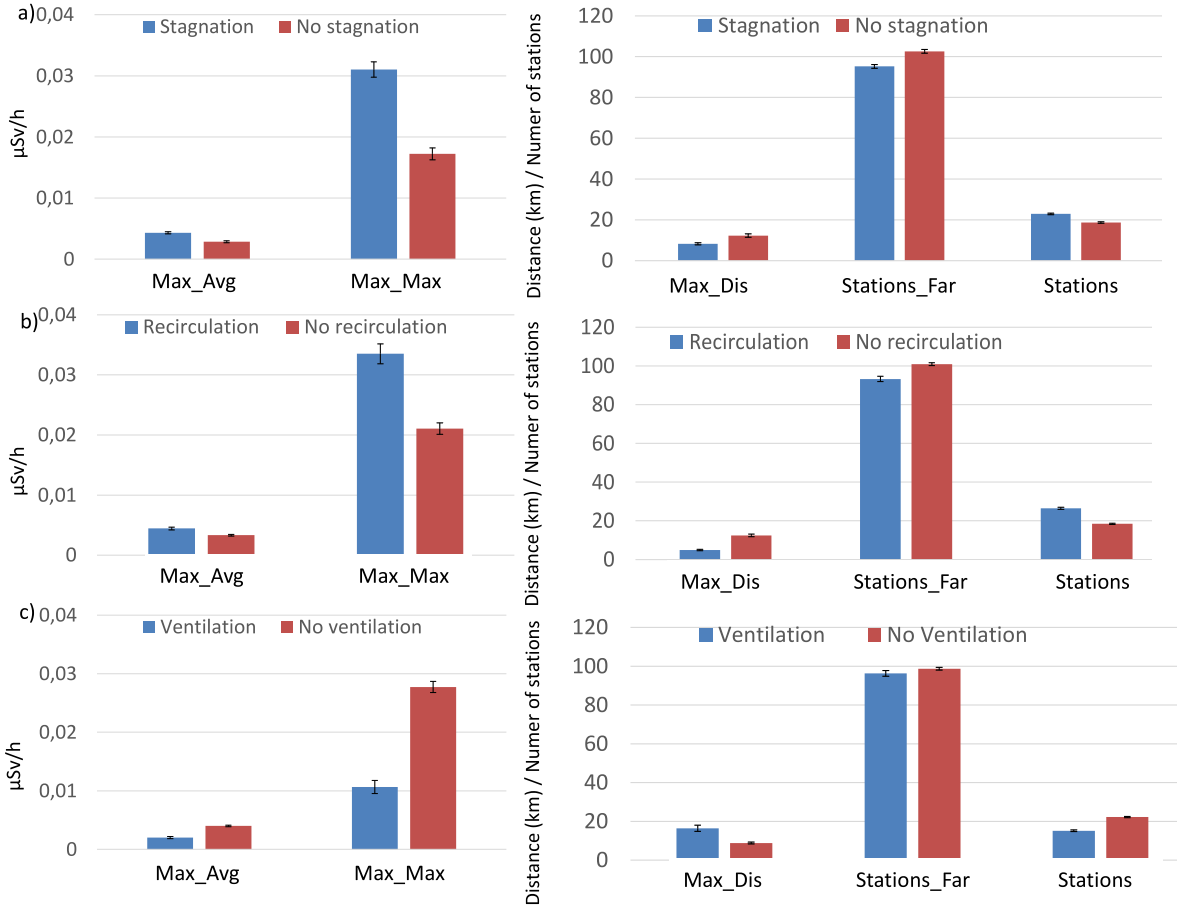

Fig. 6. Impact of a) stagnation, b) recirculation and c) ventilation processes on atmospheric dispersion parameters.

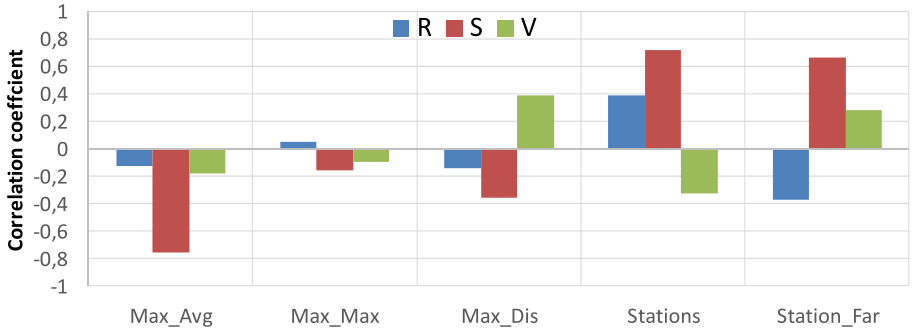

Fig. 7. Pearson correlation coefficient between the monthly averaged values of recirculation, stagnation and ventilation, and the averaged Max_Avg, Max_Max, Max_Dis,Stations, and Stations_Dis during the period 2012–2015.

parameters and atmospheric processes during the whole period (2012–2015). Taking as reference the monthly variability of each parameter and atmospheric process, stagnation negatively correlates with Max_Avg and Max_Max, indicating lower TGDR under stagnant conditions, due to limited transport. In contrast, ventilation and recirculation show weak positive correlations, suggesting minor influences on TGDR levels.

Spatial dispersion parameters (Max_Dis and Station_Far) exhibit opposing trends: ventilation enhances pollutant spread over larger distances, while stagnation restricts it. However, stagnation correlates positively with Station_Far, implying long-range transport despite lower values. Recirculation plays a limited role in maximum dispersion but primarily redistributes pollutants locally. The number of affected stations (Stations) correlates positively with stagnation and recirculation, suggesting widespread but localized impacts, while ventilation shows a weak negative correlation, indicating a more confined dispersion.

4.4. *Examples of radioactivity dispersion under extreme recirculation, stagnation and ventilation processes*

Fig. 8 illustrates the distribution of affected stations resulting from emissions under extreme conditions (maximum and minimum) of stagnation (Fig. 8a), recirculation (Fig. 8b), and ventilation (Fig. 8c), respectively, to demonstrate how each process influences the dispersion

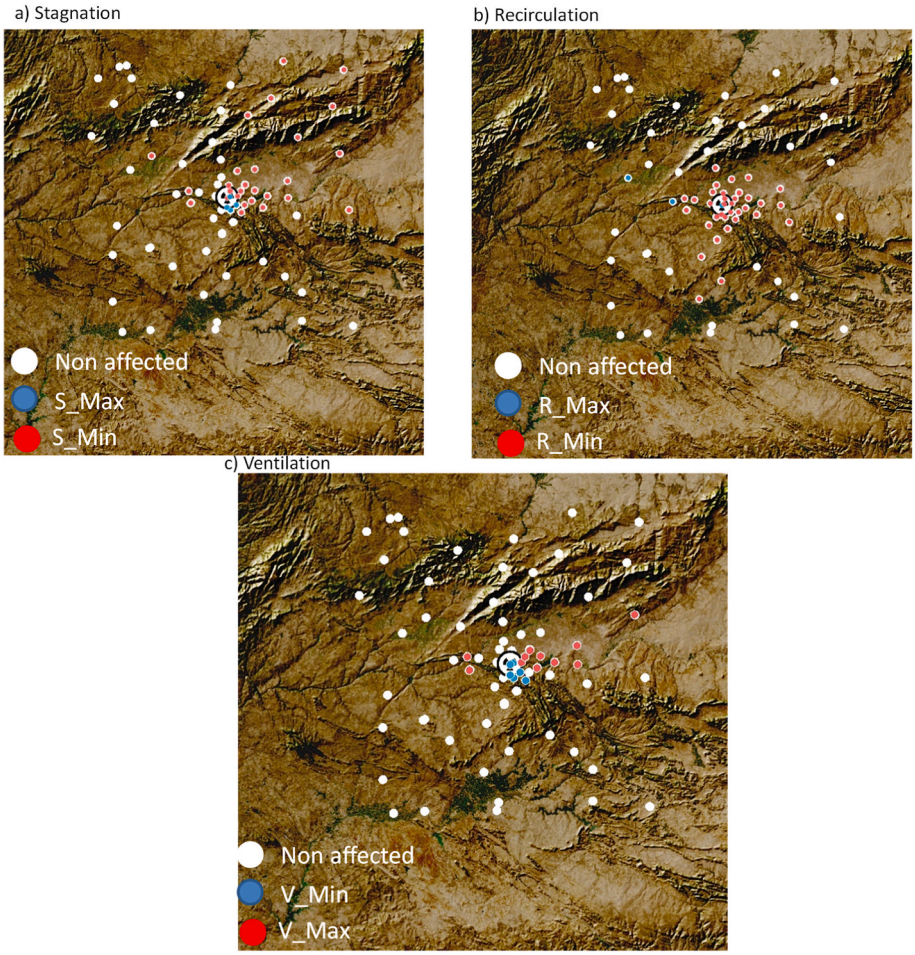

Fig. 8. Differences in the spatial distribution of monitoring stations from the source affected by plumes under a) stagnation, b) recirculation and c) ventilation processes. Each point represents one EURDEP station in Fig. 1.

of radionuclides in this specific area. Start dates of all extreme scenarios are the following: S_Max: 19/11/2012; S_Min: 12/11/2015; R_Max: 08/07/2013; R_Min: 10/12/2013; V_Max: 29/01/15; V_Min: 12/11/2015.

Fig. 8a shows a broader spatial dispersion around the release point in case of the highest stagnation, extending further from the source in both latitude and longitude. This indicates that higher stagnation levels are associated with increased potential transport of pollutants over a wider area. In contrast, under minimum stagnation conditions, the affected stations are clustered more tightly around the release point, suggesting limited pollutant movement and increased concentration near the source. Similar behaviour is obtained in the case of recirculation process (Fig. 8b), in which under maximum recirculation conditions, the affected stations are predominantly located near the release point, with a denser clustering compared to other conditions. This pattern reflects the trapping effect of strong recirculation, where air masses repeatedly cycle over the same area, leading to localized pollutant accumulation. Conversely, minimum recirculation conditions result in a slightly broader dispersion of stations and few stations affected. Finally, Fig. 8c, which compares the effects of maximum and minimum ventilation conditions, shows a notable dispersion under maximum ventilation, extending further away from the source, consistent with effective pollutant transport and dilution by strong atmospheric mixing. In contrast, minimum ventilation leads to a tighter clustering of stations near the release point, similar to the patterns observed under high stagnation and recirculation.

These results also shows that dispersion patterns are strongly influenced by the local orography, as the measurement point is located within an east-west oriented valley. The affected stations are consistently aligned along this orientation, indicating that the valley's topography plays a significant role in channeling pollutant transport. This suggests that, regardless of the prevailing atmospheric process, dispersion is also constrained by the valley's structure, reinforcing the importance of considering orographic effects in elaborating or optimizing radiological environmental impact assessment.

5. Conclusions

This study demonstrates the significant role of local wind circulation patterns—stagnation, recirculation, and ventilation—in influencing the dispersion and deposition of radionuclides following a hypothetical release from a nuclear facility. By applying these wind indices to a radiological impact assessment, the results confirm that simple meteorological parameters can provide valuable insights into the potential spread and accumulation of airborne radioactive material. The metrics used here are particularly suited to local-to-regional scales (tens to a few hundreds of kilometres), consistent with the 200 × 200 km domain considered around the ANPP. Through a series of 1256 dispersion simulations for the ANPP, the findings highlight that stagnation and recirculation conditions lead to higher radionuclide concentrations near the source, increasing the risk of local accumulation. Conversely, ventilation conditions enhance dispersion, reducing local concentrations but extending the affected area. The analysis confirms that these easily computed wind indices correlate well with transport efficiency, demonstrating their potential as practical tools for evaluating dispersion scenarios, especially for nuclear power plants located in complex terrain, where recirculation events are more likely to occur. Given their computational simplicity and predictive capability, these indices could be introduced into emergency preparedness planning. Future research should explore their application across different geographical regions and reactor types to refine their predictive value further and support the development of more adaptive nuclear safety frameworks; for instance, a systematic sensitivity analysis of different release heights (e.g. 50–200 m) would represent a relevant extension to further assess the robustness and variability of the dispersion patterns, and similarly, evaluating the influence of the inversion-layer height on radionuclide transport would provide an additional and valuable extension for improving the understanding of vertical stratification effects in complex terrains.

CRediT authorship contribution statement

M.A. Hernández-Ceballos: Writing – original draft, Methodology, Formal analysis, Data curation, Conceptualization. **M. Sangiorgi:** Writing – review & editing, Software, Methodology, Data curation. **N. Conte:** Writing – review & editing, Visualization. **J.P. Bolívar:** Writing – review & editing, Supervision.

Declaration of competing interest

The authors declare that they have no known competing financial interests or personal relationships that could have appeared to influence the work reported in this paper.

Acknowledgement

Funding for open access charge: Universidad de Córdoba/CBUA

Data availability

Data will be made available on request.

References

Adame, J.A., Bolívar, J.P., de la Morena, B.A., 2009. Surface ozone measurements in the southwest of the Iberian Peninsula (Huelva, Spain). Environ. Sci. Pollut. Control Ser. 17, 355–368.
AEMET, 2019. Recuperación de la Clasificación Sinóptica de Font: Reconstrucción con el Reanálisis ERA40. NIPO: 639-19-013-7.
Allwine, K.J., Whiteman, C.D., 1994. Single-station integral measures of atmospheric stagnation, recirculation and ventilation. Atmos. Environ. 28, 713–721, 1994.
Andronopoulos, S., Davakis, E., Bartzis, J.G., Kovalets, I., 2010. RODOS meteorological pre-processor and atmospheric dispersion model DIPCOT: a model suite for radionuclides dispersion in complex terrain. Radioprotection 45 (5), S77–S84.
Birikorang, S.A., Abrefah, R.G., Sogbadji, R.B.M., Nyarko, B.J.B., Fletcher, J.J., Akaho, E. H.K., 2015. Ground deposition assessment of radionuclides following a hypothetical release from Ghana Research Reactor-1 (GHARR-1) using atmospheric dispersion model. Prog. Nucl. Energy 79, 96–103.
Choi, J.S., Kim, J.W., Joo, H.J., Lee, J.Y., Lee, C.H., Moon, J.H., 2023. Analysis of wind field data surrounding nuclear power plants to improve the effectiveness of public protective measures. Nucl. Eng. Technol. 55, 3599–3616.
Cinelli, A., Hernandez-Ceballos, M.A., Bossew, P., Tollefsen, T., Sanchez, I., Marín-Ferrer, M., Nishev, A., Bogucarskis, K., Gruber, V., De Cort, M., 2014. Method to estimate the terrestrial component of ambient doce equivalent rate from EURDEP routine monitoring data to improve the European Geogenic Radon Map. In: 12th International Workshop GARRM (On the Geological Aspects of Radon Risk Mapping), 51. Book of Proceedings.
Elkhatib, H., Awad, M.A., El-Samanoudy, M.A., 2021. Modeling of atmospheric dispersion and radiation dose for a hypothetical accident in radioisotope production facility. Prog. Nucl. Energy 134, 103674.
García-Santiago, O., Hahmann, A.N., Badger, J., Peña, A., 2024. Evaluation of wind farm parameterizations in the WRF model under different atmospheric stability conditions with high-resolution wake simulations. Wind Energ. Sci. 9, 963–979.
He, S., Zhao, Z., Ni, S., Deng, W., Zhao, J., 2024. A CFD study on radionuclides diffusion and dose assessment in Daya Bay nuclear power plant. Prog. Nucl. Energy 173, 105271.
Hernández-Ceballos, M.A., Sangiorgi, M., Pla, P., Jackson, K., Stucic, M., Ammirabile, L., De la Rosa Blul, J.C., De Cort, M., 2023. Impact of source term release characteristics of nuclear plant on the performance of EURDEP to identify radioactive plumes. Prog. Nucl. Energy 140, 103886.
Hersbach, H., Bell, B., Berrisford, P., Hirahara, S., Horányi, A., Muñoz-Sabater, J., 2020. The ERA5 global reanalysis. Q. J. R. Meteorol. Soc. 146, 730.
Huang, Y., Song, X., Zou, S., Xu, S., Zhao, F., Liu, N., 2023. Study on the atmospheric diffusion of airborne radionuclide under LOCA of offshore floating nuclear power plants based on CALPUFF. Sustainability 15 (3), 2572.
IAEA, 2018. Prospective radiological environmental impact assessment for facilities and activities. Series: IAEA Saf. Stand. Series. ISSN 1020–525X; no. GSG-10. ISBN 978–92–0–102518–0.
Kovalets, I., Korolevych, V., Khalchenkov, A.V., Ievdin, I.A., Zheleznyak, M.J., Andronopoulos, S., 2013. Influence of the diagnostic wind field model on the results of calculation of the microscale atmospheric dispersion in moderately complex terrain. Atmos. Environ. 79, 29–35.
Levy, I., Dayan, U., Mahrer, Y., 2010. Differing atmospheric scales of motion and their impact on air pollutants. Int. J. Climatol. 30, 612–619.
Nabavi, S.O., Christoudias, T., Proestos, Y., Fountoukis, C., Al-Sulaiti, H., Lelieveld, J., 2023. Spatiotemporal variation of radionuclide dispersion from nuclear power plant

accidents using FLEXPART mini-ensemble modeling. Atmos. Chem. Phys. 23, 7719–7739.
Pinheiro, A., Desterro, F., Santos, M.C., Pereira, C.M.N.A., Schirru, R., 2017. GPU-based implementation of a diagnostic wind field model used in real-time prediction of atmospheric dispersion of radionuclides. Prog. Nucl. Energy 100, 146–163.
Russo, A., Gouveia, C.M., Soares, P.M.M., Cardoso, R.M., Mendes, M.T., Trigo, R.M., 2018. The unprecedented 2014 Legionnaires' disease outbreak in Portugal: atmospheric driving mechanisms. Int. J. Biometeorol. 62, 1167–1179.
Sangiorgi, M., Hernández-Ceballos, M.A., Bolívar, J.P., 2023. Analysing the performance of radiological monitoring network during nuclear accidents. Prog. Nucl. Energy 160, 104689.
Thykier-Nielsen, S., Deme, S., Mikkelsen, T., 1999. Description of the Atmospheric Dispersion Module RIMPUFF. Technical Report RODOS (WG2)-TN(98)-02. Forschungszentrum Karlsruhe GMBH.
von Schoenberg, P., Tunved, P., Grahn, H., Wiedensohler, A., Krejci, R., Brännström, N., 2021. Aerosol dynamics and dispersion of radioactive particles. Atmos. Chem. Phys. 21, 5173–5193.
Wang, T., Du, H., Zhao, Z., Russo, A., Zhang, J., Zhou, C., 2022. The impact of potential recirculation on the air quality of Bohai Bay in China. Atmos. Pollut. Res. 13, 101268.
Wu, S., Wang, Y., Chen, C., Cao, Z., Cao, J., Yu, Z., Song, H., 2021. Valley city ventilation under the calm and stable weather conditions: a review. Build. Environ. 194, 107668.
Yoshikane, T., Yoshimura, K., 2018. Dispersion characteristics of radioactive materials estimated by wind patterns. Sci. Rep. 8, 9926.
Yoshikane, T., Yoshimura, K., Chang, E.C., et al., 2016. Long-distance transport of radioactive plume by nocturnal local winds. Sci. Rep. 6, 36584.
Zhou, Z., Wei, G., Zheng, H., Russo, A., Li, C., Du, H., Xiang, J., 2019. Effects of potential recirculation on air quality in coastal cities in the Yangtze River Delta. Science of The Total Environment 651, 12–23.